

**INDUCED MAGNETIC PROPERTIES TO SURFACE-MODIFIED
MESOPOROUS CLAY HETEROSTRUCTURES FOR
ANTI-CORROSION PACKAGING**

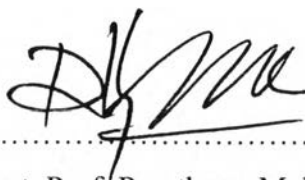
Anusara Jindapech

A Thesis Submitted in Partial Fulfilment of the Requirements
for the Degree of Master of Science
The Petroleum and Petrochemical College, Chulalongkorn University
in Academic Partnership with
The University of Michigan, The University of Oklahoma,
and Case Western Reserve University
2010

I 2837 5397

Thesis Title: Induced Magnetic Properties to Surface-Modified Mesoporous Clay Heterostructures for Anti-Corrosion Packaging
By: Anusara Jindapech
Program: Polymer Science
Thesis Advisors: Asst. Prof. Hathaikarn Manuspiya
Assoc. Prof. Rathanawan Magaraphan

Accepted by the Petroleum and Petrochemical College, Chulalongkorn University, in partial fulfillment of the requirements for the Degree of Master of Science.



..... College Dean
(Asst. Prof. Pomthong Malakul)

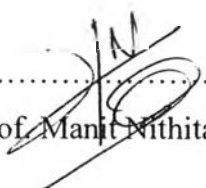
Thesis Committee:



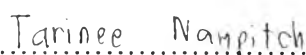
.....
(Asst. Prof. Hathaikarn Manuspiya)



.....
(Assoc. Prof. Rathanawan Magaraphan)



.....
(Asst. Prof. Manit Nithitanakul)



.....
(Dr. Tarinee Nampitch)

ABSTRACT

4872006063: Polymer Science Program

Anusara Jindapech: Induced Magnetic Properties to Surface-Modified Mesoporous Porous Clay Heterostructures for Anti-Corrosion Packaging.

Thesis Advisors: Asst. Prof. Hathaikarn Manuspiya and Assoc. Prof. Rathanawan Magaraphan 119 pp.

Keywords: Porous clay heterostructures/ Polylactide/ Nanocomposites/Vapor corrosion inhibitor

Porous clay heterostructures (PCHs) provide a large specific area that can be modified by a functional group. In this work, a PCH surface was modified by Fe (Fe^{2+} and Fe^{3+}) to obtain magnetic PCH. The various Mn ion contents were added into magnetic PCH to enhance the magnetic properties. After that, magnetic PCH was modified by a vapor corrosion inhibitor (VCI). Subsequently, these materials were blended with polylactide to yield polylactide-clay nanocomposites for anti-corrosion packaging. The results from the Surface Area Analyzer (SAA) showed that the surface area of the PCH decreased after modification. SEM images and EDX micrographs showed the successful incorporation of the Fe and Mn ion into the PCH. The saturation magnetization (M_s) increased with the higher content of Mn. Magnetic PCH (0 % Mn) can absorb the most water. The results of the TG/DTA showed that the incorporation of VCI onto the magnetic PCH led to a shift in the DTG peaks to lower temperature, suggesting the increasing volatility brought about by the incorporation on the magnetic PCH. After testing the corrosion, the magnetic PCH-40 %wt VCI has the lowest corrosion rate. The oxygen gas permeability rate was decreased in the PLA nanocomposites due to the enhancing barrier properties of the magnetic PCH.

บทคัดย่อ

อนุสรณ์ จินดาเพชร : การใช้สมบัติความเป็นแม่เหล็กเพื่อการปรับปรุงพื้นผิวของแร่ดินเหนียวที่มีรูพรุนสำหรับใช้งานเกี่ยวกับบรรจุภัณฑ์ป้องกันสนิม (Induced Magnetic Properties to Surface-Modified Mesoporous Clay Heterostructure for Anti-Corrosion Packaging) อ. ที่ปรึกษา : ผศ.ดร. หทัยกานต์ มนัสปิยะ และ รศ.ดร. รัตน์วรรณ มกรพันธุ์ 119 หน้า

แร่ดินเหนียวที่มีรูพรุนมีพื้นที่ผิวมากกว่าแร่ดินเหนียวโดยทั่วไป ซึ่งสามารถปรับปรุงพื้นผิวได้ด้วยหมู่ฟังก์ชันต่างๆ ได้ ในงานวิจัยนี้ได้ทำการดัดแปลงโครงสร้างรูพรุนของแร่ดินเหนียวด้วยอนุภาคเหล็กเพื่อให้ได้แร่ดินเหนียวที่มีสมบัติทางแม่เหล็ก และได้มีการดัดแปลงโครงสร้างรูพรุนด้วยอนุภาคแมงกานีสในปริมาณต่างๆ เพื่อปรับปรุงสมบัติทางแม่เหล็กของแร่ดินเหนียวที่มีรูพรุน หลังจากนั้นแร่ดินเหนียวที่มีรูพรุนที่มีสมบัติทางแม่เหล็กนี้ ถูกนำมาดัดแปลงโครงสร้างด้วยสารยับยั้งการเกิดสนิมอีกครั้ง ดินดังกล่าวนี้ถูกนำมาเตรียมเป็นแผ่นฟิล์มนาโนคอมพอสิตกับพอลิแลกไทด์ ซึ่งเหมาะสมที่ให้เป็นบรรจุภัณฑ์ป้องกันการเกิดสนิม จากการศึกษาการเกิดโครงสร้างรูพรุนด้วยเทคนิคการดูดซับก๊าซใน โดโรเจนพบว่าดินมีพื้นที่ผิวลดลงหลังจากมีการดัดแปลงโครงสร้างรูพรุน จากภาพถ่ายส่องกราดแบบวิเคราะห์ธาตุพบว่า มีอนุภาคเหล็กและอนุภาคแมงกานีสบนพื้นผิวของแร่ดินเหนียวที่ทำการดัดแปลงโครงสร้างแล้ว ค่าสมบัติทางแม่เหล็กของแร่ดินเหนียวที่ทำการดัดแปลงโครงสร้างนี้มีค่าเพิ่มขึ้นเมื่อมีปริมาณอนุภาคแมงกานีสเพิ่มขึ้นและแร่ดินเหนียวที่มีรูพรุนนี้สามารถดูดซับไอน้ำได้มากที่สุดเมื่อไม่มีการดัดแปลงโครงสร้างด้วยอนุภาคแมงกานีส ผลจากการศึกษาสมบัติทางความร้อนพบว่าการดัดแปลงโครงสร้างของแร่ดินเหนียวรูพรุนที่มีสมบัติทางแม่เหล็กด้วยสารยับยั้งการเกิดสนิม ทำให้พิกเคลื่อนย้ายไปทางอุณหภูมิที่ต่ำลง นั่นแสดงว่า สารยับยั้งการเกิดสนิมสามารถระเหยกลายเป็นไอเพิ่มขึ้นเมื่อมีการรวมตัวกันของสารยับยั้งการเกิดสนิมและแร่ดินเหนียวรูพรุนที่มีสมบัติทางแม่เหล็ก จากการศึกษาการเกิดสนิม พบว่าแร่ดินเหนียวรูพรุนที่มีสมบัติทางแม่เหล็กที่ดัดแปลงโครงสร้างด้วยสารยับยั้งการเกิดสนิมร้อยละสี่สิบมีอัตราการเกิดสนิมช้าที่สุด และในการศึกษาการซึมผ่านของก๊าซออกซิเจนบนวัสดุนาโนคอมพอสิตดังกล่าว พบว่าวัสดุนาโนคอมพอสิตมีค่าการซึมผ่านของก๊าซออกซิเจนน้อยกว่าพอลิแลกไทด์ เนื่องจากการเพิ่มขึ้นของคุณสมบัติการดักจับก๊าซของตัวแร่ดินเหนียวเอง

ACKNOWLEDGEMENTS

This work would not have been possible without the assistance of the following individuals.

First of all, the author would like to gratefully give special thanks to her advisors, Asst. Prof. Hathaikarn Manuspiya and Assoc. Prof. Rathanawan Magaraphan for their intensive suggestions, valuable guidance and vital help throughout this research. In addition, the author deeply thanks to Asst. Prof. Manit Nithitanakul and Dr. Tarinee Nampitch for serving on her thesis committee.

The author is grateful for the scholarship and funding of the thesis work provided by the Petroleum and Petrochemical College; Center of Excellence for Petroleum, Petrochemical, and Advanced Materials, Thailand; Polymer Processing and Polymer Nanomaterial Research Units and also National Research Council of Thailand (NRCT). The author would like to thank Optimal Technology Co, Ltd., for providing the raw materials to carry out this research.

Special thanks go to all of the Petroleum and Petrochemical College's faculties who have tendered invaluable knowledge and to the college staff who willingly gave support and encouragement.

Finally, the author would like to take this opportunity to thank PPC Ph.D. students and all her PPC friends for their friendly assistance, cheerfulness, creative suggestions, and encouragement. Also, the author is greatly indebted to her parents and her family for their support, love and understanding.

TABLE OF CONTENTS

	PAGE
Title Page	i
Abstract (in English)	iii
Abstract (in Thai)	iv
Acknowledgements	v
Table of Contents	vi
List of Tables	xi
List of Figures	xiii
Abbreviations	xvii
 CHAPTER	
I INTRODUCTION	1
 II LITERATURE REVIEW	 4
 III EXPERIMENTAL	 30
3.1 Materials	30
3.1.1 Clay Minerals	30
3.1.2 Surfactants	30
3.1.3 Co-surfactant	30
3.1.4 Silica Sources	30
3.1.5 Solvents	30
3.1.6 Polymer	30
3.1.7 Compatibilizer	30
3.1.8 Iron Source	30
3.1.9 Manganese Source	30
3.1.10 Vapor Corrosion Inhibitor	30
3.2 Equipments	31
3.2.1 X-ray Diffractometer (XRD)	31
3.2.2 Surface Area Analyzer (SAA)	31

CHAPTER	PAGE
3.2.3 Fourier Transform Infrared Spectroscopy (FT-IR)	31
3.2.4 Thermogravimetric Analysis (TGA)	31
3.2.5 Differential Scanning Calorimetry (DSC)	32
3.2.6 Scanning Electron Microscope (SEM)	32
3.2.7 Transmission Electron Microscope (TEM)	32
3.2.8 X-Ray Fluorescence Spectrometer (XRF)	32
3.2.9 Gas Permeability Tester	32
3.2.10 Water vapor Permeability Tester	32
3.2.11 Atomic Force Microscope (AFM)	33
3.2.12 Vibration Sample Magnetometer (VSM)	33
3.2.13 The Volatilization of VCI Test	33
3.2.14 The Corrosion Test	33
3.2.15 Mechanical Testing	33
3.2.16 UV/vis Spectrophotometer	33
3.2.17 Twin Screw Extruder	34
3.2.18 Compression Molding	34
3.3 Methodology	34
3.3.1 Purification and pH Adjustment of Na-Monmorillonite	34
3.3.2 Synthesis of Porous Clay Heterostructures (PCHs)	34
3.3.3 Preparation of Magnetic PCH	35
3.3.4 Preparation of Magnetic PCH-VCI	35
3.3.5 Preparation of Nanocomposites	35
 IV SURFACE-MODIFIED POROUS CLAY HETEROSTRUCTURES (PCHs) FOR THE MAGNETIC PROPERTIES ENHANCEMENT	 36
4.1 Abstract	36
4.2 Introduction	36
4.3 Experimental	37

CHAPTER	PAGE
4.4 Results and Discussion	40
A. The Interlayer Distance of Montmorillonite, Organoclay and PCH	40
B. Fourier Transform Infrared Spectroscopy (FT-IR) Analysis	41
C. Pore Characterization of PCH and Magnetic PCHs	42
D. The UV/vis Absorbance Spectra Analysis	44
E. The X-ray Fluorescence Analysis	45
F. Moisture adsorption Analysis	45
G. Vibration Sample Magnetometer	47
H. The Morphology Analysis	49
4.5 Conclusions	52
4.6 Acknowledgements	53
4.7 References	53
V THE EFFECT OF VAPOR CORROSION INHIBITOR CONCENTRATION DOPED IN MAGNETIC PCH FOR PREPARATION OF POLYLACTIDE NANOCOMPOSITES AS AN ANTI-CORROSION PACKAGING	54
5.1 Abstract	54
5.2 Introduction	54
5.3 Experimental	56
5.4 Results and Discussion	59
5.4.1 Characterization of magnetic PCH-VCI	59
A. The volatilization of PCH, Magnetic PCH and Magnetic PCH-VCI	59
B. The Corrosion Test of PCH, Magnetic PCH and Magnetic PCH-VCI	60
5.4.2 Characterization of PLA Nanocomposites	63

CHAPTER	PAGE
A. Thermal Properties of Nanocomposites	63
B. Mechanical measurement of PLA Nanocomposites	67
C. The Corrosion Test of PLA Nanocomposites	70
5.5 Conclusions	74
5.6 Acknowledgements	74
5.7 References	74
VI ANTI-CORROSION PACKAGING FABRICATED BY POLYLACTIDE/VAPOR INHIBITOR MODIFIED MAGNETIC PCH NANOCOMPOSITE	76
6.1 Abstract	76
6.2 Introduction	76
6.3 Experimental	78
6.4 Results and Discussion	81
A. Thermal Properties of Nanocomposites	81
B. Mechanical measurement of PLA nanocomposites	84
C. The Corrosion Test of PLA Nanocomposites	86
D. Dispersion of magnetic PCH in PLA nanocomposites	89
E. Surface of carbon steel in corrosion test	90
F. The structure of PLA nanocomposites	92
G. Oxygen Gas and moisture permeability of PLA Nanocomposites	94
6.5 Conclusions	95
6.6 Acknowledgements	96
6.7 References	96
VII CONCLUSIONS AND RECOMMENDATIONS	98
REFERENCES	100

CHAPTER	PAGE
APPENDICES	107
Appendix A Monmorillonite Clay, PK-810	107
Appendix B Types of Adsorption Isotherm and Hysteresis Loop	108
Appendix C Data of Mechanical Properties of PLA nanocomposites with various VCI contents	109
Appendix D Data of Mechanical Properties of PLA nanocomposites with various Magnetic PCH- 40%wt VCI contents	113
Appendix E Oxygen Gas Permeability ($\text{cc/m}^2\cdot\text{d}$) of PLA nanocomposites	116
Appendix F Moisture Permeability ($\text{g/m}^2\cdot\text{d}$) of PLA nanocomposites	117
Appendix G Data of Mechanical Properties of blown film PLA/5%wt PEG/1%wt Magnetic PCH-40%wt VCI	118
CURRICULUM VITAE	119

LIST OF TABLES

TABLE		PAGE
CHAPTER II		
2.1	Examples of common inhibitor systems classified by their modes of action	26
CHAPTER IV		
4.1	The basal spacing of montmorillonite and organoclay	41
4.2	Porosity characteristics of montmorillonite PCH and magnetic PCHs	43
4.3	Chemical Composition of PCH and Magnetic PCHs	45
4.4	Moisture adsorption (%) of PCH and Magnetic PCHs	46
4.5	Magnetization and Coercivity of Magnetic PCH with various Mn ion contents	48
CHAPTER V		
5.1	The first date of corrosion of carbon steel in PCH, Magnetic PCH, Pure VCI and Magnetic PCH-VCI	61
5.2	Thermal properties of neat PLA and PLA nanocomposites	64
5.3	Mechanical Properties of neat PLA and PLA nanocomposites	68
5.4	The first date of corrosion of carbon steel in neat PLA and PLA nanocomposites	70
CHAPTER VI		
6.1	Thermal properties of neat PLA and PLA nanocomposites	83
6.2	Mechanical Properties of neat PLA and PLA nanocomposites	84
6.3	The first date of corrosion of carbon steel in neat PLA and PLA nanocomposites	87
6.4	The basal spacing of Magnetic PCH-40 %wt VCI and various PLA nanocomposites.	93

TABLE	PAGE
6.5 Oxygen gas permeability of neat PLA, PLA/5%wt PEG and PLA nanocomposites	94
6.6 Moisture permeability of neat PLA, PLA/5%wt PEG and PLA nanocomposites	95

LIST OF FIGURES

FIGURE		PAGE
CHAPTER II		
2.1	Structure of montmorillonite.	5
2.2	Schematic representation of a cation-exchange reaction between the silicate and an alkylammonium salt.	6
2.3	Schematic representation of porous clay hetero structure (PCH) formation through surfactant-directed assembly of mesostructured silica in the galleries of a quaternary ammoniumion-exchanged layered silicate co-intercalated by an electrically neutral amine cosurfactant.	8
2.4	TEM image saponite heterostructure.	9
2.5	The skeletal formula of polylactic acid.	10
2.6	The schematic of different types of composite arising from the interaction of layered silicates and polymers: (a) phase-separated microcomposite; (b) intercalated nanocomposite and (c) exfoliated nanocomposite.	13
2.7	Schematically illustration of three different types of thermodynamically achievable polymer/layered silicate nanocomposites.	14
2.8	Grafting of mercaptopropylsilane groups to the inner and outer walls of mesostructural silica intercalated in smectite clay.	18
2.9	The schematic representation of a hysteresis loop for a ferroelectric material in an electric field.	21
2.10	The schematic of action of Vapor Corrosion Inhibitor.	25
CHAPTER IV		
4.1	The XRD patterns of (a) montmorillonite, (b) Organoclay and (c) PCH. The insertion show the XRD patterns of (b) Organoclay, and (c) PCH (zoom in).	41

FIGURE	PAGE
4.2 FTIR spectra of (a) MMT, (b) Organoclay, and (c) PCH.	42
4.3 N ₂ adsorption-desorption isotherms of montmorillonite, PCH, and magnetic PCHs.	43
4.4 UV/vis absorbance spectra of as-synthesized PCH, magnetic PCHs (Fe:Mn), and MMT.	44
4.5 Moisture adsorption of PCH, and Magnetic PCHs.	46
4.6 Magnetization curves of Magnetic PCH with various Mn ion contents.	48
4.7 SEM images of (a) Montmorillonite, and (b) PCH.	49
4.8 TEM image of (a) magnetic PCH (Fe:Mn=20:0), (b) magnetic PCH (Fe:Mn=20:0) (zoom out), and (c) magnetic PCH (Fe:Mn=20:20).	51
4.9 SEM image and consistent EDX micrograph of 5%wt Mn ion in PCH (a) SEM image, and (b) Mn mapping.	51
4.10 SEM image and consistent EDX micrograph of 20%wt Mn ion in PCH (a) SEM image, and (b) Mn mapping.	52

CHAPTER V

5.1 Volatilization before test of PCH, magnetic PCH, Pure VCI, and Magnetic PCH-VCI.	59
5.2 Volatilization after test of PCH, magnetic PCH, Pure VCI, and Magnetic PCH-VCI.	60
5.3 The carbon steel after corrosion test of (a) PCH, (b) Magnetic PCH, (c) Pure VCI, (d) Magnetic PCH-20%wt VCI, (e) Magnetic PCH-40%wt VCI, (f) Magnetic PCH-60%wt VCI, and (g) Magnetic PCH-80%wt VCI.	61
5.4 The corrosion before test of PCH, magnetic PCH, Pure VCI, and Magnetic PCH-VCI.	62
5.5 The corrosion after test of PCH, magnetic PCH, Pure VCI, and Magnetic PCH-VCI.	63

FIGURE	PAGE
5.6 DSC heating scan thermograms of neat PLA, PLA/5%wt PEG and various PLA nanocomposites (a) Glass transition temperature, and (b) Melting temperature.	65
5.7 TG-DTA curves (a), and DTG temperature peak (b) of neat PLA, PLA/5%wt PEG and PLA nanocomposites.	67
5.8 Mechanical Properties of neat PLA and PLA nanocomposites (a) Tensile Strength, (b) % Elongation at Break, and (c) Young's Modulus.	69
5.9 The carbon steel after corrosion test of nanocomposites (a) neat PLA, (b) PLA/5%wt PEG, (c) PLA/5%wt PEG/1%wt PCH, (d) PLA/5%wt PEG/1%wt Magnetic PCH-0%wt VCI, (e) PLA/5%wt PEG/1%wt Magnetic PCH-20%wt VCI (f) PLA/5%wt PEG/1%wt Magnetic PCH-40%wt VCI, (g) PLA/5%wt PEG/1%wt Magnetic PCH-60%wt VCI, (h) PLA/5%wt PEG/1%wt Magnetic PCH-80%wt VCI, and (i) PLA/5%wt PEG/1%wt VCI.	71
5.10 The corrosion before test of neat PLA and PLA nanocomposites with various VCI contents.	72
5.11 The corrosion after test of neat PLA and PLA nanocomposites with various VCI contents.	73

CHAPTER VI

6.1 DSC heating scan thermograms of neat PLA, PLA/5%wt PEG and various PLA nanocomposites (a) Glass transition temperature and (b) Melting temperature.	82
6.2 TG-DTA curves of neat PLA and various PLA nanocomposites.	83
6.3 Mechanical Properties of neat PLA and PLA nanocomposites with various Magnetic PCH-40%wt VCI content (a) Tensile Strength, (b) % Elongation at Break and (c) Young's Modulus.	86

FIGURE	PAGE
6.4 The carbon steel after corrosion test of PLA nanocomposites (a) neat PLA, (b) 1%wt Magnetic PCH-40%wt VCI, (c) 2%wt Magnetic PCH-40%wt VCI, (d) 3%wt Magnetic PCH-40%wt VCI, (e) 4%wt Magnetic PCH-40%wt VCI and (f) 5%wt Magnetic PCH-40%wt VCI.	87
6.5 The corrosion before test of neat PLA and PLA nanocomposites.	88
6.6 The corrosion after test of neat PLA and PLA nanocomposites.	89
6.7 SEM images of PLA nanocomposites (a) neat PLA, (b) PLA/5% wt PEG and (c) PLA/5% wt PEG/1% wt Magnetic PCH-40%wt VCI.	90
6.8 3D AFM images of carbon steel in corrosion test (a) before testing, (b) after testing in Magnetic PCH-20%wt VCI powder and (c) after testing in Magnetic PCH-20%wt VCI film.	92
6.9 The XRD patterns of Magnetic PCH-40 %wt VCI and various PLA Nanocomposites.	93

ABBREVIATIONS

MMT	Na-Montmorillonite
PCHs	Porous clay heterostructures
CTAB	Cetyltrimethylammonium bromide
PLA	Poly lactide
PEG	Polyethylene glycol
Magnetic PCHs	Porous clay heterostructures + n %wt of Ferric Chloride Hexahydrate + n %wt of Ferrous Chloride Tetrahydrate (+ n %wt of Manganese (II) chloride tetrahydrate)
VCI	Vapor Corrosion Inhibitor
Magnetic PCH-VCI	Porous clay heterostructures + n %wt of Vapor Corrosion Inhibitor